www.czasopisma.pan.pl PAN POLSKA AKADEMIA NAUK www.journals.pan.pl

Arch. Metall. Mater. **65** (2020), 1, 357-366

DOI: 10.24425/amm.2020.131738

VINEET TIRTH[1*], AMIR ARABI[1]

EFFECT OF LIQUID FORGING PRESSURE ON SOLUBILITY AND FREEZING COEFFICIENTS OF CAST ALUMINUM 2124, 2218 AND 6063 ALLOYS

Liquid forging alias squeeze casting gives the combined advantage of casting and forging. Optimum process parameters are important to get a cost-efficient process. In this study, four materials have been identified, which are extensively used in industries. These materials are commercially pure Al and three Al-alloys namely, 2124, 2218 and 6063. The pouring temperature and the mold temperature is maintained at 700ºC and 250ºC respectively. The materials were developed at seven pressure variations from 0 to 150 MPa. The effect of the pressure on the microstructures, porosity, and hardness has been reported. The coefficient of solubility is estimated for all materials and a polynomial relationship is found to be the best fit with the applied pressure. The pressure of 100 MPa gives better increment in hardness. The melting point and the freezing coefficient of the materials under study have been determined. A linear relationship between the pressure and the freezing time is deduced. It is observed that the solubility and the freezing coefficients depend on the pressure as well, in addition to the composition and temperature.

Keywords: Liquid Forging; Porosity; Hardness; Solubility Coefficient; Freezing Coefficient

1. Introduction

The advantage of forging and casting can be united with the intricacy of form and decent surface finish in liquid forging. An increased casting yield (>90%) may be attained as wastage is avoided in riser and gating [1-2]. In addition, the casting can be imperiled by heat treatment, joining, cutting, finishing, coating, electroplating, and another general as well as special secondary processes. Liquid forging (LF) offers superior cost advantage compared with other processes. The foundation of liquid forging initiated in 1878 by Russian researchers who used steam pressure on molten metal while it solidified in the mold [3]. Conventionally, forging and casting have advanced distinctly but Plyastska in 1930, explored the opportunity to combine the two methods. The parameters related to the combined processes controlling the technique were efficaciously determined in the 1960s and thereafter-liquid forging was ready for commercial applications. However, the response of metals and alloys to LF depends on a number of factors and progressive research is required to design optimum process parameters. Subsequently, the LF technique became popular by the name of squeeze casting and its commercial application started on a large scale in the US, Europe, and Japan in the late 1960s [4]. At first, about one hundred and fifty large batch industries started using liquid forging in Russia, producing more than 200 engineering components being used explicitly in the automobile, aerospace and defense industries [4-10]. The method can be mechanized with reasonably modest equipment giving decent manufacture rate, dimensional replication, and finish, minimizing the machining. The liquid forging process is different from pressure die casting however, it fills the gap amid pressure die casting, gravity casting and forging. Fig. 1 shows a comparative study of liquid forging and other similar methods based on productivity. The figure has been plotted by extracting the data and results from the literature review [2-5,7-10,11,12-17].

LF hence integrates the benefits of all the three processes and yields the properties not obtainable in any of these processes separately. Two different types of LF techniques are used viz. direct and indirect [18]. In the direct LF, the molten metal is solidified under the direct pressure. The pressure is maintained until the metal or alloy solidifies so that the porosity is minimized. In this process, isotropic properties are obtained and the quality and finish of the product are good [5].

Another process is in-direct LF, in which, metal is injected into the die cavity by a small hole when the plunger applies the pressure during freezing [18]. This technique is a hybrid

[1] ASSOCIATE PROFESSOR, MECHANICAL ENGINEERING DEPARTMENT, COLLEGE OF ENGINEERING, KING KHALID UNIVERSITY, ABHA-61411, ASIR, KINGDOM OF SAUDI ARABIA

* Corresponding author: v.tirth@gmail.com, vtirth@kku.edu.sa

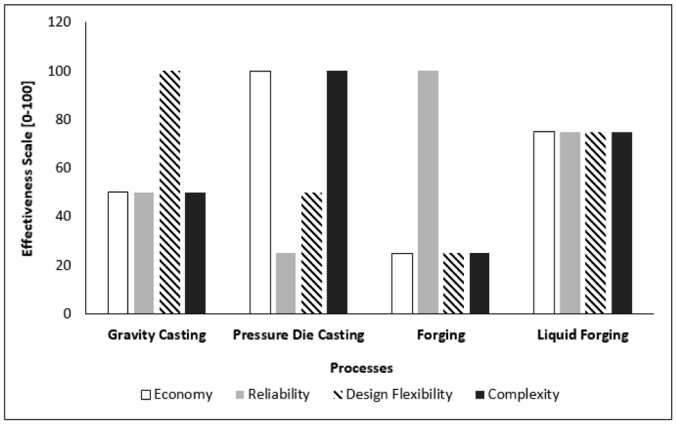

Fig. 1. Comparative study of Liquid Forging and other methods based on the effectiveness on a scale 0-100

process between low pressure die casting and the high pressure die casting. The indirect process has two disadvantages. Firstly, the riser and runner is required and secondly, it is difficult to obtain a defect-free casting. Hence, the direct process is preferred over the indirect process for the processing of materials, which are to be used for high-end applications such as in automotive, aerospace, and defense industries. The sole advantage of the indirect process is good dimensional control due to the closed die approach.

Aluminum (Al) and its alloys have vast applications in the industry. A summary of the literature review based on the studies on Al and its alloys is given in the following section.

Pressure affects the solidus as well as the liquidus temperatures of metals and alloys. During melting, the liquid and solid phases co-exist in equilibrium, higher pressures increase the transition temperature for a change in phase from solid to liquid, thereby increasing the quantity (volume) of solid to transform into a liquid at this higher temperature and reducing the temperature range from the start of melting to its completion. The addition of alloying elements further alters (normally reduces) the melting point of the alloy. During solidification, the application of pressure produces an undercooling of the melt and enhances the heat transfer through the mold surface by reducing the gap between the melt-mold surface (which hinders heat transfer) resulting in faster solidification. The increase in the cooling rate results in faster solidification, which may be evaluated by the examination of microstructures. A decrease in the size of dendrite cells, as well as the spacing between secondary dendrite arms and the reduction in grain size, is indicative of melt undercooling and faster nucleation. Pressure applied during freezing also helps in limiting the porosity by hindering the nucleation of gas bubbles, increasing the dissolution of gases in the melt and reducing the size of gas bubbles to pin holes [2,8,9,17].

In the LF process, the pressure increases the freezing rate of the metals and alloys [2]. The heat transfer between the mold-casting interface was observed to increase with the rise in pressure from 0 to 150 MPa, increasing the cooling rate, inhibiting eutectic precipitates, and reducing the size of α-Al. The pouring temperature, as well as the pressure, played a decisive role in increasing the tensile strength and elongation of the alloy [19]. Applying pressure in the semisolid state resulted in improved abrasive wear performance by 20% in matrix alloy and by 25-30% in composites. A moderate pressure of 100 MPa was recommended to obtain reasonable casting without significant microstructural problems like porosity [20-21]. For hard materials, the post solidification working is quite difficult. To achieve high hardness, it was recommended to apply pressure during the semisolid state [22-23]. To achieve the fastest cooling rate, it is desirable to obtain peak heat flux between the casting and mold surface. The peak heat flux was observed at around 5 seconds after pouring [24]. In a study to investigate the effect of pressure and pouring temperature on the microstructure and properties in 2024 Al alloy, a pouring temperature of 700°C at a pressure of 140 MPa produced sound properties [11].

The microstructure refinement results due to a reduction in grain size, as well as a reduction in the arm spacing of primary and secondary dendrites. In a study on A380 alloy, the secondary dendritic arm spacing was recorded 30% less in squeeze cast specimen prepared at 50 MPa, compared with the gravity cast specimen [25]. The pressure not only refines the structure but it also offers a favorable effect on the T6 heat treatment response of the alloy, observed in Al-11%Si T6 alloy prepared at 120 MPa [26]. The discontinuities were reduced and the interfacial reactions were observed to be faster in AZ91D/$Al_{18}B_4O_{33}$w metal matrix composites fabricated at high pressures [27]. At high pressure (320 MPa), it was observed that the mechanical properties improve significantly however, the pressure does not affect the type of phases formed during heat treatment. The refinement in microstructure increases the number and reduces the size of the precipitates [28] but, it is an energy intensive process. If a similar effect may be obtained at low pressure with a combination of other process parameters, the LF process may be optimized to obtain cost efficiency.

A study on $AlZn_6Ni_4Mg_2Cu$ alloy prepared by sand casting, permanent mold casting, and squeeze casting confirmed the grain refinement and increased precipitation of the Al_3Ni phase which were responsible for the strengthening mechanisms of the alloy. The squeeze cast samples outperformed others [29]. The extent of microstructure refinement and the precipitation of intermetallic phases differ with composition and so a study that may present a comparative analysis of the effect of pressure on the microstructure, considering the composition will be useful for the researchers and industries. During remelting the Al alloys, shrinkage porosity is reported to increase. The LF technique is recommended to control the shrinkage porosity, observed in A359 cast composites prepared by remelting of the alloy [30]. The frequency, as well as the size of shrinkage porosity, was reduced as the pressure was increased [31].

The porosity results when the gas bubbles fail to dissolve in the melt and instead they tend to nucleate. It would be interesting to obtain the relationship between porosity and the gas solubility in the melt.

The process parameters of LF, their intermediate effects and the end results are given in Table 1.

TABLE 1

Process variables of LF, the intermediate effects and results

LF Variables	Intermediates	End Results
Pressure	Grain size	Hardness
Pouring Temp	Porosity	Tensile Strength
Mold temp	Precipitates	Ductility
Press speed (not significant)	DAS	Casting yield
Dwell time (not significant)	Freezing time	
Pressure Application time		

The present work aims at the comparative study of the effect of pressure on commercially pure Aluminum (CP-Al) and three of its alloys, which are popularly used in the industry but their comparison has not been reported in published research. It is desirable to optimize the LF process parameters for cost efficiency. The alloys identified for this study are 2124 which is one of the widely used alloys in the automotive industry, 2218 alloy, which has the potential for elevated temperature applications in automotive and aerospace industries and 6063 alloy, which is a commonly used in extruded applications, mainly in structural and architectural domains. The four materials identified for investigation have been prepared by forging in a liquid to semisolid state at different pressure, the range of which has been selected on the basis of the literature review [2,11,32].

2. Materials and Methods

2.1. Materials

The elemental analysis of the materials, determined by Inductively Coupled Plasma Atomic Emission Spectrophotometer (ICP-AES) are given in Table 2, along with the codes assigned to the materials.

TABLE 2

Composition and codes assigned to the materials

Material	Code	Composition [wt%]
Commercially Pure Aluminium (CP-Al)	Al	Co-0.01, Si-0.5, Fe-0.07, Zn-0.03, Mn-0.01, Cu-0.06, Pb-0.06, Al-98.54
2124 Al-alloy	2124	Cu-4.26, Si-0.95, Mg 0.49, Fe 0.25, Mn 0.98, Ni 0.34, Al-92.73
2218 Al-alloy	2218	Cu-4.24, Ni-1.91, Mg-1.53, Fe-0.7, Sn-0.4, Mn-0.01, Pb-0.04, Cr-0.02, Al-91.15
6063 Al-alloy	6063	Si-0.32, Fe-0.35, Cu-0.1, Mn-0.1, Mg-0.64, Cr-0.1, Zn-0.95, Ti-0.9, Impurities-0.15, Al-96.39

2.2. Methods

Standard melting practices were used in preparing the material using permanent steel molds for normal casting and heat-treated chromium-molybdenum alloy steel fabricated by the authors, for LF. Based on the recommendations of published research [2,11,32], the pouring temperature was fixed at 700±5°C and the mold temperature at 250±5°C. Overall evaluation indicates that the direct method of LF is better than the indirect method to obtain high strength, defect-free casting [5,18] and so; the direct method was used. Since ambient temperature may interfere in the cooling rate, freezing time and effective mold and pouring temperatures, all the castings have been done in a temperature controlled laboratory, with the ambient temperature maintained between 25-28°C.

The pressure applied during LF may be categorized into three classes; low (<50 MPa), moderate (50-150 MPa) and high (>150 MPa). In a pilot study by the authors, a moderated pressure of 100 MPa was found suitable for considerable refinement of microstructure and limiting the porosity. The forging pressure was varied in the present study from 0 to 150 MPa in a step of 25 MPa each, using a vertical semi-automatic hydraulic press. The displacement of the plunger was measured using a dial gauge of capacity 25 mm and least count of 0.01 mm. the time of forging was measured by a stopwatch with least count of 0.01 s. Higher pressure may lead to a costly and energy-intensive process. Microstructures were examined on Olympus-PME3 digital optical microscope coupled with Axiovision image analysis software. Scanning electron studies were done on Jeol JSM-6390 LV. The etching of the samples was done using dilute (10%) Hydrofluoric acid (HF). To get the indication of mechanical properties, hardness was estimated by Vicker's hardness tester machine at 5 kg load applied for 10 s as per ASTM E92.

The porosity in the cast metals and alloys deteriorate the properties and also interferes in the secondary processing. The porosity was carefully measured by first determining the density of the CP-Al and the alloying elements by water immersion method as per ASTM C 135-96 standard. A cylindrical sample of 6 mm diameter and 10 mm height of each material was taken. The densities of the block of materials were determined by Eq. (1).

$$\rho_c = \frac{(M_a)}{M_a - M_w} * d_w \tag{1}$$

Where ρ_c is the density of the cast material, M_a is the mass in gm of the material in air, M_w is the mass in gm of the material in distilled water and d_w is the density of distilled water at ambient temperature.

The weighing balance used for determining the mass of the material was Citizen make, with a least count of 0.001 gm. The porosity was estimated by Eq. (2).

$$V_p = \frac{M_c}{\rho_c} - \left(\left[\frac{M_x}{\rho_x} \right] + \left[\frac{M_y}{\rho_y} \right] + \left[\frac{M_z}{\rho_z} \right] + \ldots \right) \tag{2}$$

Where V_p is the volume of porosity, M_c is the mass of casting and ρ_c is the density of the casting. M_x, M_y, M_z, etc. represent the mass of alloying elements obtained by multiplying the mass fraction of the elements with the mass of cast alloy sample and ρ_x, ρ_y, ρ_z, etc. are the densities of the alloying elements determined from Eq. (1). The density of the elements present as an impurity or in

very small amount has been taken from the periodic table. The average of at least three readings was considered as the density.

It is a known fact that the pressure increases the solubility of gases in a liquid, relationship of solubility with the pressure is given by Eq. (3) [17].

$$C_s = K_s\sqrt{p} \tag{3}$$

Where C_s is the solubility of gases in a liquid, p is the applied pressure during solidification and K_s is the solubility coefficient depending upon the composition and temperature of the melt. The solubility of the gases in the melt has been taken as the reciprocal of porosity, estimated from Eq. (4), and the value of the solubility coefficient K_s has been determined for all four materials under investigation, at all seven forge pressures using Eq. (5).

$$C_s = \frac{1}{V_p} \tag{4}$$

$$K_s = \frac{\frac{1}{V_p}}{\sqrt{p}} \tag{5}$$

The freezing time of metal or alloy may be estimated by Eq. 6 [33].

$$t = K_f \ln\left[\left(T_p - T_m\right)/\left(T_l - T_m\right)\right] \tag{6}$$

Where t is the time for freezing, K_f is the freezing coefficient depending upon the composition and temperature of the metal or alloy, T_p is the pouring temperature, T_m is the mold temperature, T_l is the melting point.

If one determines the solidification time t, having known the other temperatures in Eq. (6), the value of freezing coefficient K_f may be determined by Eq. (7).

$$K_f = \frac{t}{\ln\left[\left(T_p - T_m\right)/\left(T_l - T_m\right)\right]} \tag{7}$$

In this study, the feezing time is referred as the time interval of piston movement after it came in contact with the melt and when it ceases to move, measured by a stopwatch with a least count of 0.01 sec. The displacement of the piston was determined by a dial gauge with a least count of 0.01 mm and a capacity of 25 mm. The time and displacement measurement was commenced with the start of load on the semi-automatic hydraulic press and was measured to the point where the piston displacement ceased. The value of freezing coefficient K_f has been determined for CP-Al and 2124, 2218, and 6063 alloys using Eq. (7).

The melting points of the materials have been determined by recording time-temperature data in a resistance furnace with two Type K Alumel/Chromel thermocouples, one inserted in the muffle and the other in the graphite crucible, in contact with the material. The furnace was calibrated with the boiling point of distilled water. A day before melting of the materials, the furnace and the crucible were preheated to 300°C to remove moisture. The material was placed in the crucible only after the temperature reached 100°C. After melting, the liquid was superheated to 700°C before pouring. The thermocouple recording the temperature of the material was placed such that it was completely dipped in the liquid melt. The crucible was placed in the middle of the furnace in the highest heating zone. Thermocouples were also placed in the same zone.

3. Results and Discussion

3.1. Micrography

All the four materials under investigation were prepared at seven forge pressures (0, 25, 50, 75, 100, 125 and 150 MPa). The etched optical micrographs of the specimen of CP-Al, 2124, 2218 and 6063, prepared at 100 MPa are represented in Fig. 2 from (a) to (d) respectively. The microstructures have been over-etched, if required, to reveal the details. In Fig. 2(a), the α-Al appear as bright patches. The crystal growth is enclosed in dashed circles. Porosity is marked by white circles. Grains are distinctly visible, the grain boundaries are marked by arrows.

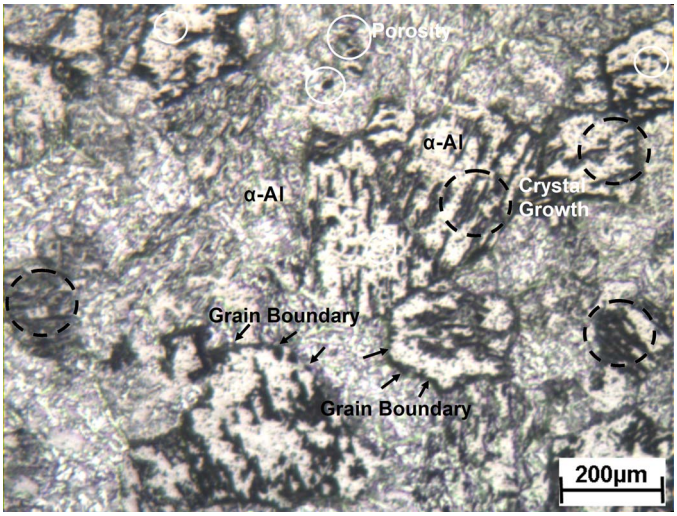

Fig. 2(a). Optical micrographs (etched) of CP-Al prepared at 100 MPa

In 2124, shown in Fig. 2(b), the porosity is marked inside the white circles, the square boxes highlight the dross, dendrite cell boundaries are marked with solid arrows and intermetallic precipitates are marked with dashed arrows.

The 2218 alloy has contrasting dendrite cell boundaries, marked with solid arrows in Fig. 2(c). The porosity is marked in circles and the intermetallic precipitates, visible in light shade, are marked with dashed arrows. The bright region is α-Al. The matrix indicates some dark patches due to over-etching.

Fig. 2(d) represents the 6063 alloy. Dross is enclosed in the square boxes, porosity in white circles and the grain boundaries are marked with arrows. All the micrographs are at the same magnification. While comparing them, it is observed that there is excessive dross formation in 6063, probably due to the presence of Zn, which is a low melting point element. The refinement of

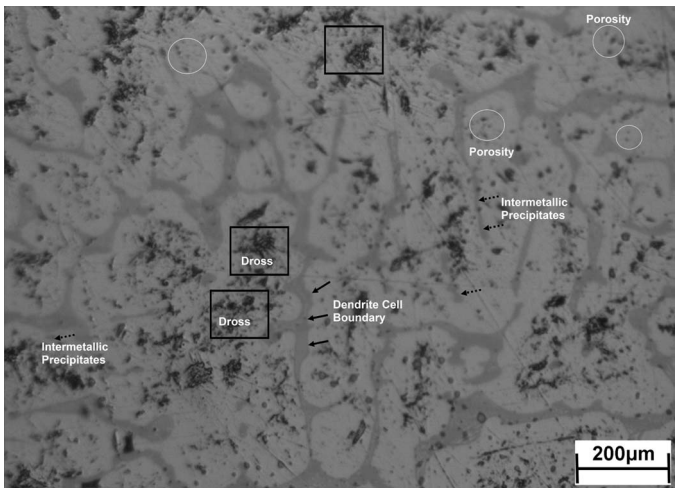

Fig. 2(b). Optical micrographs (etched) of 2124 prepared at 100 MPa

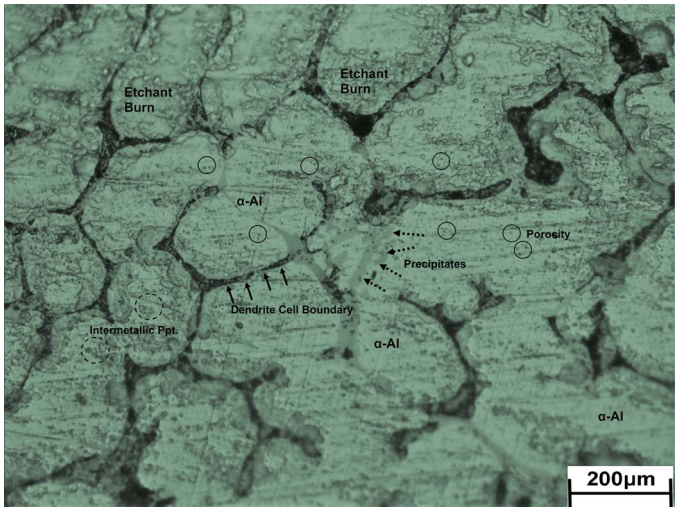

Fig. 2(c). Optical micrographs (etched) of 2218 prepared at 100 MPa

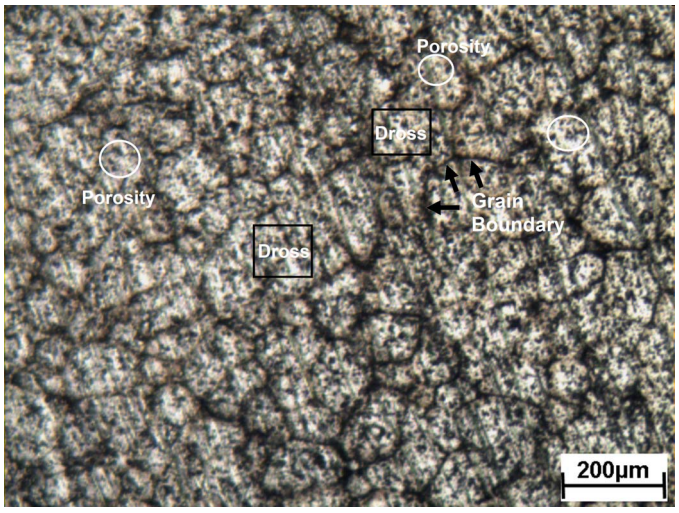

Fig. 2(d). Optical micrographs (etched) of 6063 prepared at 100 MPa

the structure appears to be the best in 2124 alloy, followed by 6063, 2218 and Al. This gives an indication that the intermetallic precipitates promote grain nucleation. The thick dendrite cell boundaries in 2124 and 2218 alloy may have resulted due to the segregation of the precipitates. There has been a sharp response to etching by 6063, due to which the structure appears quite dark.

The SEM pictures of the materials Al, 2124, 2218 and 6063, prepared at 100 MPa are represented in Fig. 3 from (a) to (d) respectively. In Fig. 3(a), the porosity is marked in white circles, the shrinkage porosity is marked in the box, the grain boundaries are marked by the arrows. Some inclusions are also present which may be the particles of the crucible material or dust.

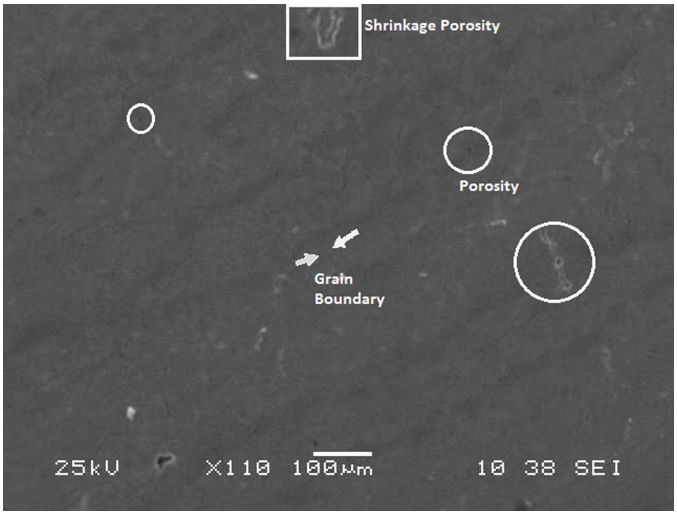

Fig. 3(a). SEM pictures of CP-Al prepared at 100 MPa

In Fig. 3(b) (2124 alloy), the porosity is marked inside circles and the grain boundaries are marked by arrows. The intermetallic precipitates are well distributed in the matrix. Some inclusions are distinctly marked in the box.

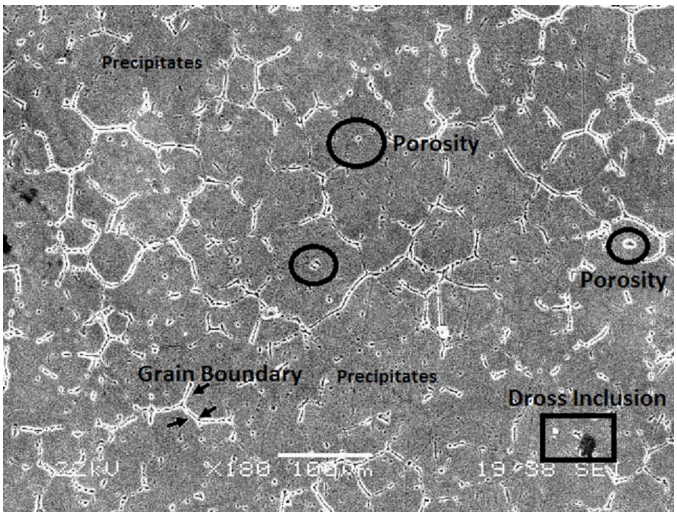

Fig. 3(b). SEM pictures of 2124 prepared at 100 MPa

Fig. 3(c) represents 2218 alloy. The α-Al phase is observed, surrounded by the dendrite cells, marked with solid arrows. The intermetallic precipitates are marked with dashed arrows and the shrinkage porosity is marked in circles.

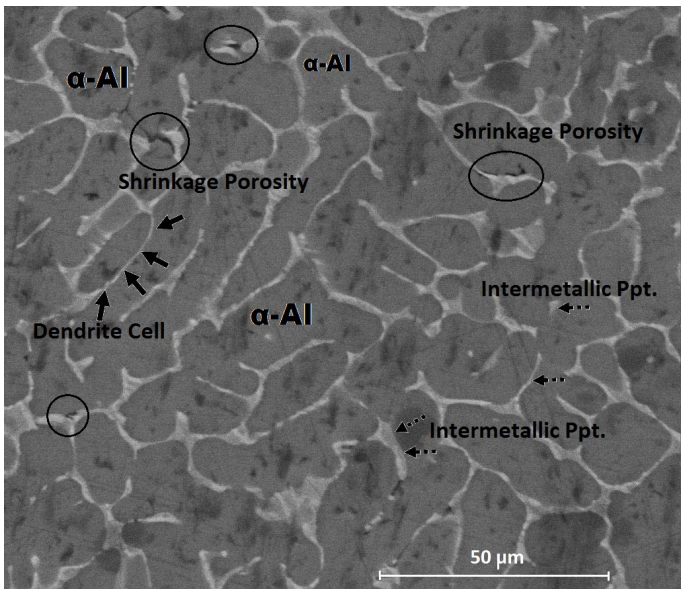

Fig. 3(c). SEM pictures of 2218 prepared at 100 MPa

Fig. 3(d) shows the porosity highlighted in circles, the grain boundaries, intermetallic precipitates, and some inclusions. All the SEM pictures clearly reveal the microstructural details, porosity is apparently high in 2124 alloy followed by 6063, 2218 and appears to be minimum in Al. It is apparent from the microstructures that the intermetallic precipitates result in higher porosity, hindering the dissolution of the gas bubbles in the liquid and their diffusion along the melt. Some inclusions are visible in all the materials. The grains appear more circular in 2124 alloy and their refinement may be observed in all the materials. The effect of applied pressure during solidification is known to refine the microstructure of metals, alloys, and composites. Published literature reveals that as the pressure was increased from 0 to 220 MPa, the grains size of 2218-Al_2O_3(TiO_2) composite was reduced by about 50% [8]. The dendrite arm spacing was reduced by 62.5% when Al-Al_2O_3-MgO composite was forged at a pressure of 140 MPa [34]. The dendrite cells were observed to become more round as the forge pressure was increased [10].

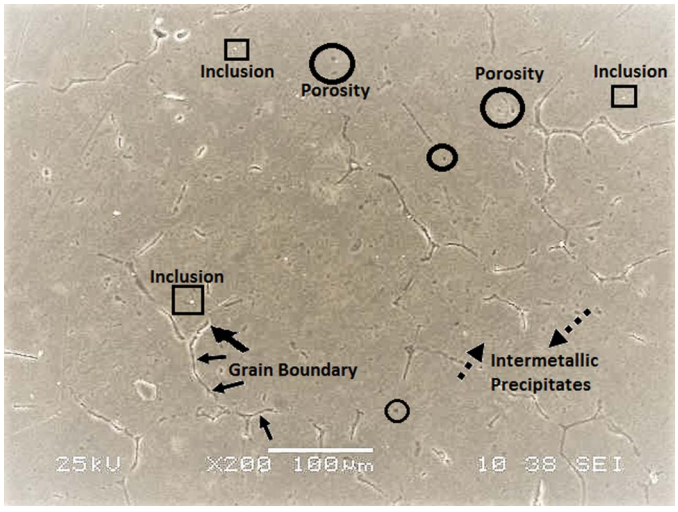

Fig. 3(d). SEM pictures of 6063 prepared at 100 MPa

At ambient pressure, the grains were observed to be elongated and as the pressure was applied during the solidification, the grains became circular [9-10].

3.2. Solubility Coefficient K_S

The porosity is a function of pressure, greater the pressure, less is the porosity. Fig. 4 shows the porosity at seven forge pressures for the materials under investigation. The porosity reduces with the rise in pressure in all the materials. The absorbed gases and moisture from the atmosphere often results in porosity in the metals and alloys. These gas bubbles nucleate during solidification but if the solidification happens under pressure, the solubility of the gases increase, resulting in a reduction in the evolution of gases during freezing and hence reducing the porosity. Therefore, as the pressure is increased from 0 to 150 MPa, porosity is found to decrease in all the materials. The porosity is reduced by 58.94% in CP-Al, 55.55% in 2124, 52.38% in 2218, and 54.4% in 6063. The reduction in porosity is slightly higher in CP-Al due to the absence of the intermetallic precipitates which may act as the favorable sites for retention of pores and hinder there dissolution or diffusion. The reduction in porosity is of the same order in all the three alloys. Slightly higher porosity in gravity cast 2124 and 6063 alloys may be due to the presence of more number of precipitates and higher dross, observed from the optical microstructures in Fig. 2(b) and (d). Formation of dross may have resulted in entrapment of a larger amount of air or moisture from the atmosphere.

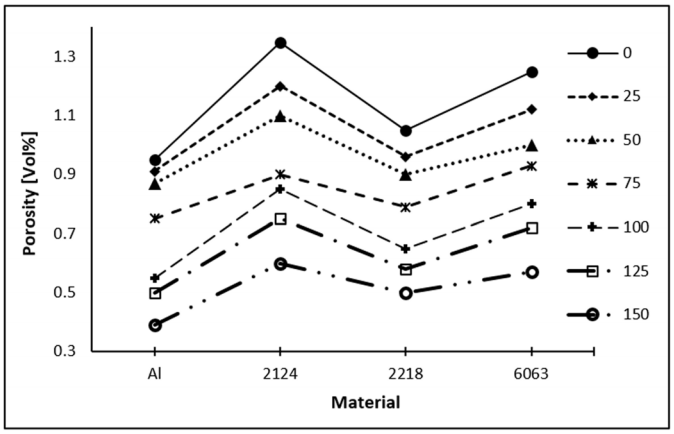

Fig. 4. The porosity in materials CP-Al, 2124, 2218, and 6063 prepared at 0, 25, 75, 100, 125 and 150 MPa

The solubility coefficient K_s has been estimated for all the four materials at all seven forge pressures and plotted in Fig. 5. It is observed that the solubility coefficient K_s, which has been reported to be a function of composition and temperature of the melt, also depends on the pressure. The solubility coefficient K_s varies from 0.117 to 0.219 in the materials under investigation. It first decreases with the increase in pressure and then increases due to the combined effect of cooling, pressure, and the refinement of microstructure. During freezing, there is a change in the

composition due to the precipitation of phases, which may have also contributed to this trend. The polynomial equations are found to be the best fit, relating the coefficient K_s with pressure p for all the materials. The equations have been derived from the trends of the plot and are given as follows.

$$K_{Al} = e^{-5}p^2 - 0.0023p + 0.2588 \quad (8)$$

$$K_{2124} = 8e^{-6}p^2 - 0.0016p + 0.1989 \quad (9)$$

$$K_{2218} = e^{-5}p^2 - 0.002p + 0.2443 \quad (10)$$

$$K_{6063} = e^{-5}p^2 - 0.002p + 0.22 \quad (11)$$

Where K_{Al}, K_{2124}, K_{2218} and K_{6063} are the solubility coefficients (K_s) for Al, 2124, 2218 and 6063 respectively and p is pressure. Using these equations, the pressure required for desired solubility (or porosity) of gases may be calculated to design LF process for metals or alloys. Since the experiments have been conducted only on four materials, the average value of coefficient K_s may be taken for other alloys of Al, which is 0.155 and it may be validated in future research.

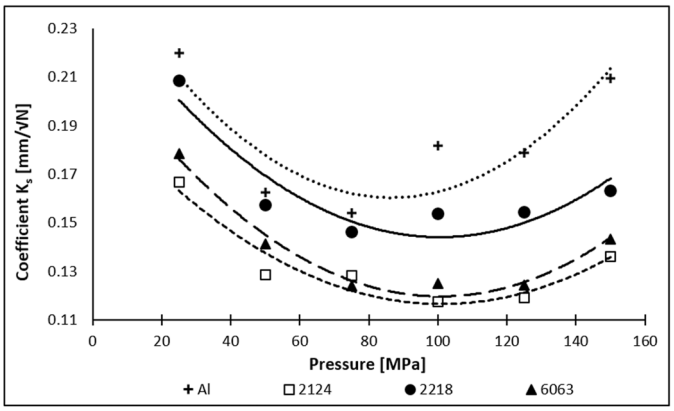

Fig. 5. Coefficient K_s in materials CP-Al, 2124, 2218, and 6063 prepared at 0, 25, 75, 100, 125 and 150 MPa

3.3. Hardness

Hardness is a primary mechanical property, which influences the other properties namely, strength, wear etc. The hardness of the materials prepared under different pressures is plotted in Fig. 6. The hardness improves with pressure for all the materials. The pouring temperature and the die temperature were maintained at 700°C and 250°C respectively to limit porosity and obtain microstructure refinement, derived from literature review and pilot study. It is expected that the variations in hardness may change if the pouring temperature and the die temperatures are changed, however; this variation was not included in the scope of the study. The percent improvement in hardness from its value at 0 MPa is also given on Fig. 6. The improvement in hardness varies from 12.84% (in 2124) to 22.58% (in Al). The precipitates in the alloys improve the base hardness and so the improvement in hardness achieved after the application of pressure is less in alloys, compared to CP-Al. Higher hardness in 2218 may be attributed to less porosity and improved precipitation of intermetallic phases.

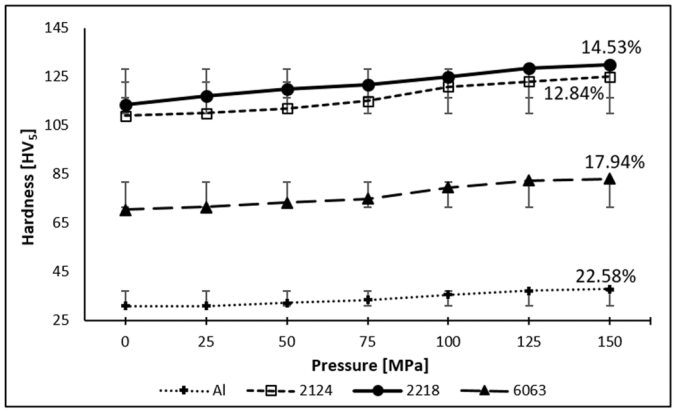

Fig. 6. Hardness [HV_5] of materials Al, 2124, 2218, and 6063 prepared at 0, 25, 75, 100, 125 and 150 MPa. The digit in % indicates improvement in hardness from its value at 0 MPa

The improvement in the hardness at each step compared with the preceding pressure is presented in Fig. 7. In each step of 25 MPa, the improvement in hardness is observed. A minimum of 0.91% and a maximum of 6.86% improvement in the hardness is recorded. One may clearly observe that the percent improvement in hardness is maximum when the pressure is increased from 75 to 100 MPa, these observations justify the recommendations that a moderate pressure of 100 MPa yields a reasonably refined microstructure of the materials within the boundaries of research design.

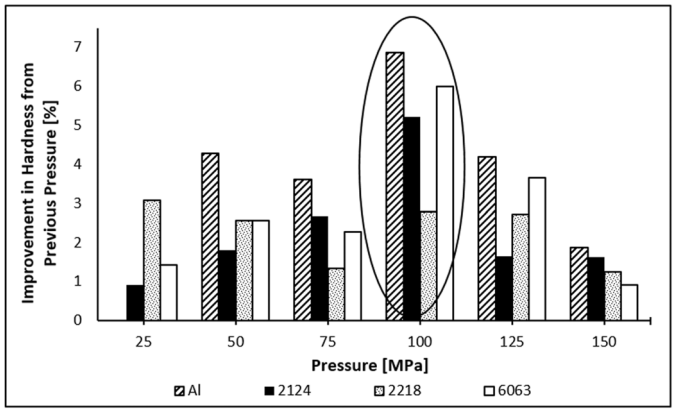

Fig. 7. Improvement in hardness (%) from the preceding pressure

3.4. Freezing Coefficient K_f

The freezing process of pure materials is normally isothermal but for alloys, freezing happens over a range of temperature, deviating from the isothermal trend. To study the freezing process, a time-temperature curve was plotted, shown in Fig. 8(a) and (b). The temperatures were measured with thermocouples embedded in the muffle as well as in close contact with the material. The desired superheat of the melt

was obtained between 215-225 minutes for all the materials. A difference of 50-60°C is observed between the temperature of the muffle and the temperature of the melt, due to the presence of air (insulator) in between the muffle and the crucible. The temperature of muffle, as well as the temperature of the material, increased steadily from 100°C, as seen in Fig. 8(a) until a point where the plot became stagnant for about 20-30 minutes in the materials, this is the temperature when the materials started absorbing the latent heat and the melting starts. This region of stagnation is almost horizontal in CP-Al as it is expected to melt at a constant temperature. However, for the alloys, this stagnation appears to be isothermal for a short period and this temperature is recorded as the melting point of the material. In Fig. 8(b) this region of stagnation is enlarged and shown. T_l is marked as the melting points of the materials. Table 3 summarizes the melting point of the materials measured in the study along with the solidus-liquidus temperature range, (obtained from literature) [35-38]. After a certain time, the temperature starts rising in all the material which indicates that the melting is complete and the sensible heating has started. This sensible heating is continued until the desired superheat temperature (700°C) is achieved.

TABLE 3

The melting point of the materials

Material	Melting Point [°C]	Solidus-Liquidus Range [°C] [35-38]
CP-Al	641.6	660.3 (Pure Al)
2124	538.5	502-638
2218	598.3	502-638
6063	621.8	616-654

For calculations, the mold temperature is taken as 250°C and the pouring temperature is taken as 700°C. The freezing time of materials is plotted with forging pressure in Fig. 9. The maximum freezing time was observed for Al, followed by 6063, 2218, and 2124. The freezing time declines almost linearly with the increase in forging pressure. The slope of the CP-Al is slightly more than the other materials, due to lesser impurities and better thermal conductivity. The equations of freezing time t with forging pressure p have been obtained from best fitting curve (in this case, linear) and given by Eq. (12), to (15) for Al, 2124, 2218, and 6063 respectively. These equations may be used to calculate the freezing time for the materials, even beyond the range of pressures employed in the study.

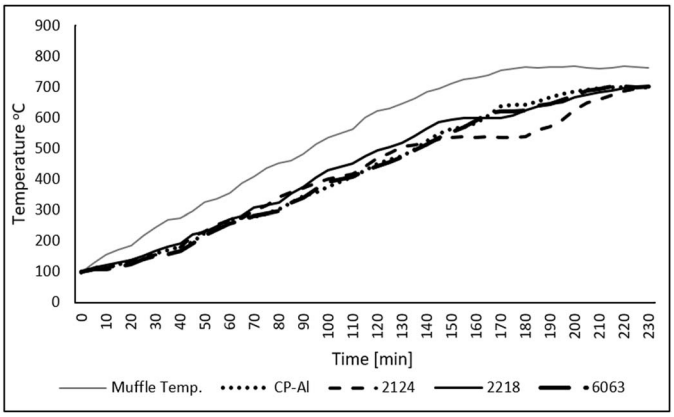

Fig. 8(a). Time-Temperature diagram of the muffle and the materials

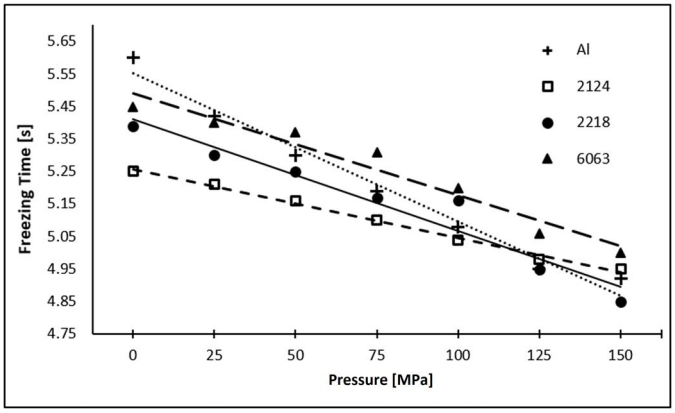

Fig. 9. Freezing time [s] of materials CP-Al, 2124, 2218, and 6063 prepared at 0, 25, 75, 100, 125 and 150 MPa

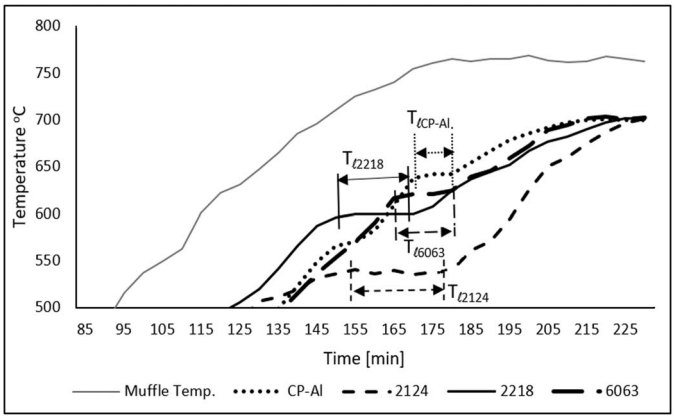

Fig. 8(b). Time-Temperature diagram enlarged, reflecting the melting of materials

$$t_{Al} = -0.1143p + 5.6657 \quad (12)$$

$$t_{2124} = -0.0529p + 5.31 \quad (13)$$

$$t_{2218} = -0.0861p + 5.4971 \quad (14)$$

$$t_{6063} = -0.0786p + 5.57 \quad (15)$$

The freezing coefficient K_f has been estimated using Eq. (7) and the data has been plotted for all the four materials at all the pressures in Fig. 10. The average value of K_f is shown on the plot in digits. This coefficient hence is dependent on the pressure as well, in addition to the composition and temperature. It is inferred that the K_f depends on the melting point, if T_l is high, as, in the case of Al and 6063, K_f is high as well.

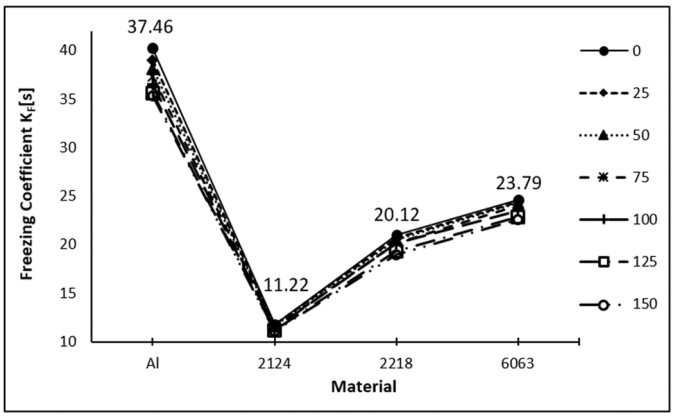

Fig. 10. Coefficient K_f of materials Al, 2124, 2218, and 6063 prepared at 0, 25, 75, 100, 125 and 150 MPa. The digits show the average value of K_f for a material

4. Conclusions

Four materials were developed at seven forge pressures in a step of 25 MPa from 0 to 150 MPa to investigate the effect of pressure on microstructure and relationship coefficients K_s and K_f. The values of these coefficients have been determined for the four materials and their relationship with pressure has been established experimentally using curve fitting. At moderate pressure of 100 MPa, the microstructures are refined with a limited presence of porosity. Dendrite cells and intermetallic precipitates are well distributed in the alloys. Porosity reduced with the increase in pressure, the best response is observed in CP-Al, indicating that the presence of precipitates hinders the dissolution or diffusion of gas bubbles. Solubility coefficient K_s was reported to be a function of composition and temperature. In this study, it is observed that it has a complex dependence on the pressure as well, following the polynomial trend. K_s varies from 0.117 to 0.219, within the pressure range of 0-150 MPa with an average value of 0.155, which may be used is further studies on Al alloys. The hardness improves with pressure from 12.84% to 22.58%. CP-Al shows a better response to the pressure. At a pressure of 100 MPa, the percent improvement in hardness is better in all materials. The melting points of the materials are 641.6°C (Al), 538.5°C (2124), 598.3°C (2218), and 621.8°C (6063). The relationship between the freezing time and pressure for all the materials was developed and reported. The freezing coefficient K_f was estimated for all the materials at all seven pressures. The variation, as well as the average value, was reported, which the researchers may use for Al alloys to estimate required parameters.

Acknowledgment

Authors thankfully acknowledge the funding and support provided by Deanship of Scientific Research, King Khalid University, Abha-Asir, Kingdom of Saudi Arabia, with grant number G.R.P.-321-40 to complete the research work.

REFERENCES

[1] S.N. Chou, J.L. Huang, D.F. Lii, H.H. Lu, J. Alloys Compd. **419**, 98 (2006).
[2] M. Dhanashekar, V.S.S. Kumar, Procedia Eng. **97**, 412 (2014).
[3] M.T. Abou EI-Khair, Mater. Lett. **59**, 894 (2005).
[4] X. Fang, S. Lü, L. Zhao, J. Wang, L. Liu, S. Wu, Mater. Design. **94**, 353 (2016).
[5] C.G. Kang, K.S. Yun, Fabrication of metal-matrix composite by the die-casting technique and the evaluation of their mechanical properties, J. Mater. Process Tech. **62**, 116 (1996).
[6] Y. Liu, Z. Zheng, C. Yang, D. Zhu, W. Chen, Tribol. Lett. **65**, 39 (2017).
[7] V. Tirth, J. Tribol. **140**, 1 (2018).
[8] V. Tirth, S. Ray, M.L. Kapoor, Metall. Mater. Trans. A Phys. Metall. Mater. Sci. **40**, 1246 (2009).
[9] V. Tirth, A. Algahtani, E.R.I. Mahmoud, Mater. Express. **8** (6), 475 (2018).
[10] V. Tirth, A. Algahtani, A. Edacherian, Mater. Express. **8** (6), 531 (2018).
[11] A. Jahangiria, S.P.H. Marashi, M. Mohammadaliha, V. Ashofte, J. Mater. Process Tech. 245, 1 (2017).
[12] P.G.C. Manjunath, A. Kumar, M.B. Parappagoudar, J. Manuf. Process. **32**, 199 (2018).
[13] Y. Wang, S. Zhao, C. Zhang, Trans. Nonferrous Met. Soc. China, **28** (2), 235 (2018).
[14] L. Natrayan, M.S. Kumar, K. Palanikumar, Mater. Res. Express **5**, 1(2018).
[15] Q. Zhao, Y. Wu, W. Rong, K. Wang, L. Yuan, X. Heng, J. Magnes. Alloy. **6** (2), 197 (2018).
[16] F. Wang, W. Meng, H. Zhang, Z. Han, Trans. Nonferrous Met. Soc. China. **28** (10), 1920 (2018).
[17] Y. Zou. Phase equilibria and solidification of Al rich Al-Cu-Mg alloys. In: PhD Thesis. University of Wisconsin, Madison USA, 1997.
[18] T.M. Yue, G.A. Chadwick, Jr. of Mat. Proc. Tech. **58**, 302 (1996).
[19] R. Pastircak, J. Scury, Arch. Metall. Mater. **62** (4), 2193 (2017).
[20] M. Lagiewka, Arch. Metall. Mater. **59** (2), 707 (2014).
[21] F. Hnilica, V. Ocenasek, I. Stulikova, B. Smola, Kovove Mater. **43**, 300 (2005).
[22] K. Solek, P. Kapranos, Arch. Metall. Mater. **61** (4), 1901 (2016).
[23] K. Solek, S. Szczepanik, Arch. Metall. Mater. **60** (4), 2613 (2015).
[24] S.N. Kulkarni, D.K. Radhakrishna, Mater Sci-Poland. **29** (2), 135 (2011).
[25] H. Murat Lus, Kovove Mater. **50**, 243 (2012).
[26] H. Barhoumi, S. Souissi, M. ben Amar, F. Elhalouani, Kovove Mater. **54**, 249 (2016).
[27] W.G. Wang, K.C. Chang, K. Matsugi, G. Sasaki, Mater. Trans. **49** (3), 637 (2008).
[28] L. Hao, X. Yang, S. Lu, X. Fang, S. Wu, Materials Science & Engineering A. **707**, 280 (2017).
[29] D.H. Chen, Z. Chen, X.R. Zhu, Y.Y. Wu, Z.M. Guo, H.X. Shi, Rare. Metal. Mat. Eng. **46** (11), 3525 (2017).
[30] A. Klasik, M. Maj, K. Pietrzak, A. Wojciechowski, J. Sobczak, Arch. Metall. Mater. **61** (4), 2123 (2016).

[31] S. Li, K. Mine, S. Sanakanishi, K. Anzai, Mater. Trans. **48** (8), 2186 (2007).

[32] S. Venkatesana, M.A. Xaviorb, Materials Today: Proceedings **5**, 11175 (2018).

[33] B. Sh, X. Sh, L. Tian, N. Zhao, L. Li, Trans. Nonferr. Met. Soc. China **97**, 412 (2013).

[34] J. Singh, S.K. Goel, V.N.S. Mathur, M.L. Kapoor, AFS Transaction **99**, 815 (1991).

[35] http://www.matweb.com/search/datasheet.aspx?bassnum=AMEAL00

[36] http://www.matweb.com/search/datasheet.aspx?matguid=19ddeefbcbb74c0aa557e4cfcfcb0797

[37] http://www.matweb.com/search/datasheet.aspx?matguid=47278d3d797941b99c7e73f1cd890317

[38] http://asm.matweb.com/search/SpecificMaterial.asp?bassnum=MA6063T6